Compute and Visualize Discontinuity Among Neighboring Integral Curves of 2D Vector Fields

Lei Zhang[1], Robert S. Laramee[2], David Thompson[3], Adrian Sescu[3] and Guoning Chen[1]

Abstract This paper studies the discontinuity in the behavior of neighboring integral curves. Discontinuity is measured by a number of selected attributes of the integral curves. A variety of attribute fields are defined. The attribute value at any given spatio-temporal point in these fields is assigned the attribute of the integral curve that passes through this point. This encodes the global behavior of integral curves into a number of scalar fields in an Eulerian fashion, which differs from the previous pathline attribute approach that focuses on the discrete representation of individual pathlines. With this representation, the discontinuity of the integral curve behavior now corresponds to locations in the derived fields where the attribute values have sharp gradients. We show that based on the selected attributes, the extracted discontinuity from the corresponding attribute fields may relate to a number of flow features, such as LCS, vortices, and cusp-like seeding curves. In addition, we study the correlations among different attributes via their pairwise scatter plots. We also study the behavior of the combined attribute fields to understand spatial correlation that cannot be revealed by the scatter plots. Finally, we integrate our attribute field computation and their discontinuity detection into an interactive system to provide exploration of various 2D flows.

1 Introduction

Vector field analysis is a ubiquitous approach that is employed to study a wide range of dynamical systems for applications such as automobile and aircraft engineering, climate study, and earthquake engineering, among others. There is a large body of work on generating a reduced representation for the understanding of large-scale and

---

[1] University of Houston, Houston, TX, U.S.A., e-mail: `lzhang38,gchen16@uh.edu` ·

[2] Swansea University, Wales, UK, e-mail: `rlaramee@gmail.com` ·

[3] Mississippi State University, Mississippi State, MS, U.S.A., e-mail: `dst,asescu@cavs.msstate.edu`
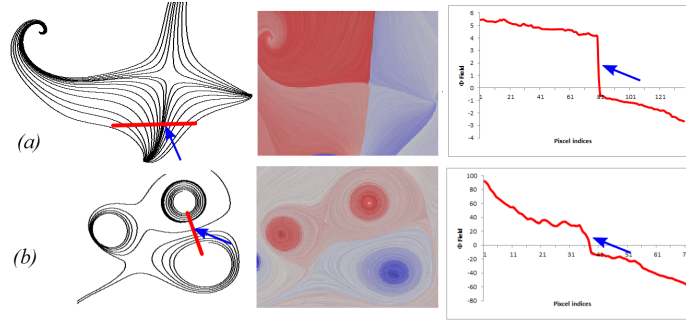
Fig. 1: The illustration of the relation between the attribute field and a number of well-known flow features, including the flow separation (a) and vortices (b). The left column shows the vector fields illustrated by streamlines, the middle column shows the rotation field, while right column shows the plots of the rotation field of the streamlines intersecting with given seeding line segments (shown in red). Note that the discontinuities (sharp gradients) in the rotation field indicate the flow features.

complex flow by classifying the integral curves based on their individual attributes. These methods typically first classify the integral curves into different clusters based on their similarity [9], then compute the representative curves for each cluster [24]. Due to the discrete representation of these methods, there is no guarantee that important flow features will be captured.

In this paper, we introduce a number of attribute fields that encode the global behaviors of the individual integral curves measured by certain geometric and physical properties. The scalar attribute value at each spatio-temporal position is derived from the attribute value of the integral curve that passes through it. With this Eulerian representation, spatio-temporal positions correlated by the same integral curves will have similar attribute values, while those neighboring points traversed by integral curves that possess rather different behaviors will have largely different attribute values. Fig. 1 provides a number of example attribute fields. The 1D plots (Fig. 1 right) show the attribute values along the seeding line segments (i.e., the red segments in Fig. 1 left) . They exhibit some cliff-like sharp changes (highlighted by the blue arrows), which correspond to certain *discontinuity* in their corresponding attribute fields. This discontinuity may be closely related to certain flow features, as flow separation indicated in Fig. 1.

We consider a number of scalar attributes as discussed in [17, 11]. To study the correlation between the attribute fields generated from these attributes, we compute their pairwise scatter plots (Fig. 5). Our results indicate that some attribute fields are highly correlated. Therefore, the set of attribute fields can be reduced. This echoes the results of [11]. More importantly, we find that the magnitude of the gradients of the attribute fields that measures the amount of change between neighboring positions exhibit strong correlation with the FTLE fields of the same flows. This coincides with the results reported in [18]. Furthermore, we compute a *super attribute field* that combines different attribute fields to study their spatial correlation. That is, we see whether two attribute fields have similar configurations (e.g., local extrema, ascending and descending trends) at the same spatial positions.

Finally, we integrate the attribute field computation and the discontinuity detection into an interactive system to support the exploration of various flow behavior via the visualization of the discontinuity structure of a chosen attribute field or the derived super attribute field. We have applied our framework to a number of synthetic and real-world 2D vector fields to demonstrate its utility.

2 Related Work

There is a large body of literature on the analysis and visualization of flow data. Interested readers are encouraged to refer to recent surveys [4, 12] that provide systematic classifications of various analysis and visualization techniques.

Among many vector field analysis techniques, vector field topology is a powerful tool that provides a streamline classification strategy based on the origin and destination of the individual streamlines. Since its introduction to the visualization community [7], vector field topology has received extensive attention for the identification of different topological features [2, 19, 23]. Recently, Morse decomposition [3] and combinatorial vector field topology [13] have also been introduced for a more stable construction and representation of vector field topology. The theory and computation of vector field topology does not apply to unsteady flows. Users usually opt for the identification of *Lagrangian Coherent structures (LCS)*, i.e., places where the flow flux is negligible, as an alternative. LCS can be extracted as the ridges of the *Finite Time Lyapunov Exponent (FTLE)* of the flow [5, 16]. Similar to these conventional flow structure analysis, our method also aims to reveal certain flow structure that indicates the boundaries of individual flow regions with different behaviors measured by specific integral curve attributes.

Salzbrunn and Scheuermann introduced *streamline predicates* that classify streamlines by interrogating them as they pass through certain user-specified features, e.g., vortices [15]. Later, this approach was extended to classify pathlines [14]. At the same time, Shi et al. presented a data exploration system to study different characteristics of pathlines based on their various attributes [17]. Pobitzer et al. demonstrates how to choose a representative set of pathline attributes for flow data exploration based on a statistics-based dimension reduction method [11]. McLoughlin et al. [10] introduced the streamline signature, based on a set of curve-based attributes, to guide the effective seeding of 3D streamlines. Different from the above integral curve classification and selection techniques that treat the individual integral curves as discrete units, our method derives a number of scalar fields throughout the entire flow domain to encode the global behaviors of integral curves. This allows us to study the discontinuity in the behaviors of neighboring integral curves via some well-established edge detection techniques, such as the Canny edge detector [1] and a discrete gradient operator.

3 Vector Field Background and Trajectory Attributes

Consider a 2-manifold $\mathbb{M} \subset \mathbb{R}^2$, a vector field can be expressed as an ordinary differential equation (ODE) $\dot{\mathbf{x}} = V(\mathbf{x}, t)$ or a map $\varphi : \mathbb{R} \times \mathbb{M} \to \mathbb{R}^2$. There are a number of curve descriptors that depict different aspects of the translational property in vector fields.

- A *streamline* is a solution to the initial value problem of the ODE system confined to a given time t_0: $\mathbf{x}_{t_0}(t) = \mathbf{p}_0 + \int_{t_0}^{t} V(\mathbf{x}(\eta); t_0) d\eta$.
- *Pathlines* are the paths of the massless particles released in the flow domain at a given time t_0: $\mathbf{x}(t) = \mathbf{p}_0 + \int_{t_0}^{t} V(\mathbf{x}(\eta); t_0 + \eta) d\eta$.
- A *streakline*, $\tilde{s}(t)$, is the connection of the current positions of the particles, $\mathbf{p}_{t_i}(t)$, that are released from position p_0 at consecutive time t_i.

There are a number of features in *steady flows*, $V(\mathbf{x})$, that are of interest. A point $\mathbf{x}_0$ is a *fixed point* (or *singularity*) if $V(\mathbf{x}_0) = 0$, and a trajectory is a *periodic orbit* if it is closed. Hyperbolic fixed points, periodic orbits and their connectivity define the *vector field topology* [2]. *Vortices* are another important flow feature that is of interest to domain experts. There is no unified definition for vortices. Informally, a vortex is a region where the flow particles are rotating around a common axis (reduced to a point in 2D). In this work, we consider streamlines with larger winding angles than a user-specified threshold, say 2π, to be within vortices. In unsteady flows, topology is not well-defined. One typically looks for certain *coherent structures* that correspond to structures in the flow that are present for a *relatively* long time. The LCS, i.e., the ridges of the FTLE field, is one such coherent structure [5]. Another feature is singularity path that depicts the trajectory of a singularity in an unsteady flow [22].

3.1 Attribute Fields

Consider an integral curve, $\mathscr{C}$, starting from a given spatio-temporal point $(\mathbf{x}, t_0)$, the attribute field value at this point is computed as:

$$\mathscr{F}(\mathbf{x}, t_0) = \mathscr{F}(\mathscr{C}(\mathbf{x})|_{t_0}^{t_0+T}) \qquad (1)$$

where $\mathscr{C}(\mathbf{x})|_{t_0}^{t_0+T}$ denotes an integral curve, i.e., either a streamline, a pathline, or a streakline starting at time t_0 with an integral time window $[t_0, t_0 + T]$. $\mathscr{F}(\cdot)$ indicates certain attribute of interest of $\mathscr{C}$. Note that, for the rest of the paper, we consider only forward integration of the integral curves. Backward integration can be considered similarly. In practice, an integral curve $\mathscr{C}$ is represented by N integration points P_i and $(N-1)$ line segments (P_i, P_{i+1}). We then define a number of attribute fields based on Eq. (1) using the integral curves attributes discussed in [11, 17].

The attribute fields we investigated in this paper with their abbreviation are rotation field Φ, length field $Ł$, average particle velocity field $avgV$, non straight velocity

field *nsV*, relative start end distance Field *seDist*, average direction field *avgDir*, acceleration *acce*, curl, Hunt's Q Q and λ_2. Fig. 3 provides a number of attribute fields derived from the Double Gyre flow. Specifically, the rotation field Φ describes the accumulated winding angle changes along the integral curves, which is defined as $\Phi_{\mathscr{C}} = \sum_{i=1}^{N-1} d\theta_i$, where $d\theta_i = (\angle(\overrightarrow{P_iP_{i+1}}, \overrightarrow{X}) - \angle(\overrightarrow{P_{i-1}P_i}, \overrightarrow{X})) \in (-\pi, \pi]$ represents the angle difference between two consecutive line segments. $\overrightarrow{X}$ is the X axis of the XY Cartesian space. $d\theta_i > 0$ if the vector field at P_i is rotating counter-clockwise with respect to the vector field at P_{i-1}, while $d\theta_i < 0$ if the rotation is clockwise. Fig. 1 provides a number of example Φ fields. The computation of the other attribute fields can be performed using a similar accumulation process based on their definitions [10, 16].

2D and 3D attribute fields If the attribute field is computed based on streamlines, it is a 2D field. Fig. 4(b) shows the rotation field of a synthetic steady flow based on streamlines. To visualize the attribute fields, we utilize a blue-white-red color coding scheme with blue corresponding to negative values and red for positive values. Pathlines or streaklines-based attribute fields are 3D fields. That is, given any spatio-temporal position $(\mathbf{x}, t_0)$, its attribute value is determined by the pathline (or streakline) starting from this position and following the forward flow direction (Eq. 1). Fig. 2 (upper) shows a volume rendering of the pathline-based Φ field of the Double Gyre flow [16] within the time range $[0, 10]$. For the rest of the paper, we focus on the behaviors of the attribute fields at specific time steps, i.e., the cross sections of the 3D field (Fig. 2 (bottom)). Fig. 3 shows a

Fig. 2: The volume rendering (upper) of the pathline-based Φ field of the Double Gyre flow. The bottom shows one slice at $t = 5$.

number of attribute fields of the Double Gyre flow. Note that the average direction field *avgDir*(Fig. 3(b)) measures the angel of between the vector pointing from the starting point to the end point of an integral curve and X axis. The range of *avgDir* field is $[0, 2\pi)$. The pathline tracing starts at $t = 0$ with integral time window size $T = 10$. Fig. 3(e) shows a Φ field computed based on the streaklines of the Double Gyre flow.
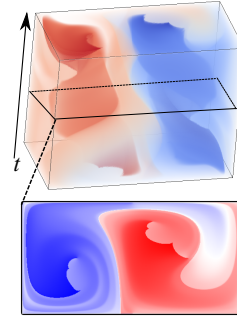
3.2 Discontinuity in Attribute Fields

3.2.1 Discontinuity Extraction

As shown in Fig. 1, the attribute fields may contain discontinuity that corresponds to the sharp gradients in the integral curve behavior. This discontinuity in the attribute fields has certain similarity to the edges in a digital image. The gradient of the attribute field may be able to locate this discontinuity (Fig. 4(f)), but may require
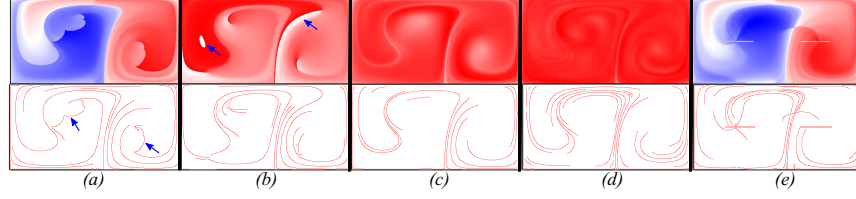
Fig. 3: Illustration of a number of attribute fields derived from the Double Gyre flow and their detected edges. (a)–(d) show the attribute fields Φ, Ł, *avgDir* and *acceration*, *avgDir* computed from pathlines, respectively. (e) is the rotation field Φ from streaklines. The parameters of Canny edge detector are $\sigma = 2.0$, $\alpha = 0.3$, $\beta = 0.8$.
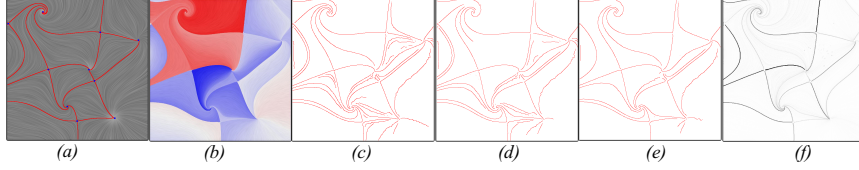

Fig. 4: Discontinuity detection from a Φ field of a synthetic steady flow using the Canny edge detector with different combinations of parameters. (a) The differential topology with LIC as the background; (b) Φ field; (c-e) Detected edges with different parameters of the Canny edge detector: (c) - $\sigma = 3.0$ $\alpha = 0.3$ $\beta = 0.8$, (d) - $\sigma = 3.0$ $\alpha = 0.6$ $\beta = 0.8$, (e) - $\sigma = 3.0$ $\alpha = 0.3$ $\beta = 0.86$; (f) The gradient of Φ field.

non-intuitive thresholds to reveal the salient ridges. Therefore, we opt for the more robust Canny edge detector [1] to locate this discontinuity from the attribute fields, which can be converted to some 2D images. The Canny edge detector has three input parameters: σ - the standard deviation of the Gaussian smoothing filter, α - the low threshold and β - the high threshold. Fig 3 bottom shows the detected edges from the corresponding attribute fields of the Double Gyre flow. Not that for the average direction field *avgDir*, the field values of the two neighboring pathlines may be (or be close) 0 and 2π respectively, as highlighted with the arrows in Fig. 3(b). But it does not indicate the discontinuity because they are the same (or the close) direction. Therefore this case is filtered out in the Canny edge detector.

3.2.2 Relation to Flow Features

Steady flow features Many discontinuities (i.e., edges identified by the edge detector) of these attribute fields share some similarity with certain well-known flow features. For example, Fig. 4 compares the discontinuity structure of the rotation field Φ of a synthetic steady flow to its topology (Fig. 4(a)), which is illustrated via a set of integral curves that end or start from saddles, i.e., *separatrices*–a special type of streamline. The Φ field is not continuous across the separatrices if the accumulation is performed using an infinite time window. This is because an arbitrarily small perturbation in the direction other than the flow direction will result in another integral curve with length much different from the separatrix, making the Φ field accumulated using Eq.(1) discontinuous at separatrices. With different param-

eters, different levels of details of the discontinuity in the Φ field can be revealed (Fig.s 4(c)-(e)). Fig. 4(f) shows the gradient of the Φ field, which does not provide a clean discontinuity structure.

LCS Lagrangian Coherent Structure (LCS) is defined as the ridges of the corresponding FTLE field. It indicates the regions of the domain with relatively large separation. Compared to LCS, it appears that the edges detected from all the attribute fields of the Double Gyre flow encode at least part of this information. This is also true for the other data sets that we have experimented with (i.e., Fig. 10 and Fig. 11). The discontinuity may be observed at the ridges of transportation, i.e., LCS due to a similar reason to the separatrices in steady flow. A pathline seeded on the ridges may have different behaviors from its neighboring pathlines caused by the separation, leading to the discontinuity in the obtained attribute fields.

Cusp seeding curves The cusp seeding curve has been discussed in [21] to reduce self-intersecting pathlines in the pathline placement. These cusp seeding curves of the Double Gyre flow can be identified from the discontinuity of the rotation field Φ as shown in Fig. 3(a). This cusp-like behavior in pathlines is caused by the abrupt change in the pathline direction, i.e., almost π angle difference between the previous and current directions, which is in turn caused by the intersection of the pathlines with the paths of singularities.

Singularity path Singularity paths reveal the trajectories of fixed points in the unsteady flows. Among all the attribute fields studied, only the Φ field computed based on streaklines encodes such information. See Fig. 3(e) for an example where the paths of the two vortices of the Double Gyre flow are revealed by the edges detected from the streakline-based Φ field. This is because singularity paths will induce the cusp-like behavior in pathlines (Fig. 12), also discussed in [21]. This cusp-like behavior corresponds to a large local angle change, which in turn leads to a large change, i.e., discontinuity in the Φ field. In addition, the temporal behavior, i.e., the moving of the singularities can only be captured by measuring the attributes of the particles released at the same position but consecutive times, i.e., streaklines.

4 Correlation Among Different Attribute Fields

Considering the large number of attributes that can be used to describe various flow behaviors, it will be interesting to see how their corresponding attribute fields are correlated. In this section, we study their correlation using two approaches, i.e., the correlation study via their pairwise scatter plots and the spatial correlation study via certain combined attribute fields.

4.1 Correlation Study Via Pairwise Scatter Plots

There are different attributes that can be used to characterize the behaviors of integral curves, as discussed in [11]. To understand their correlation, we construct a
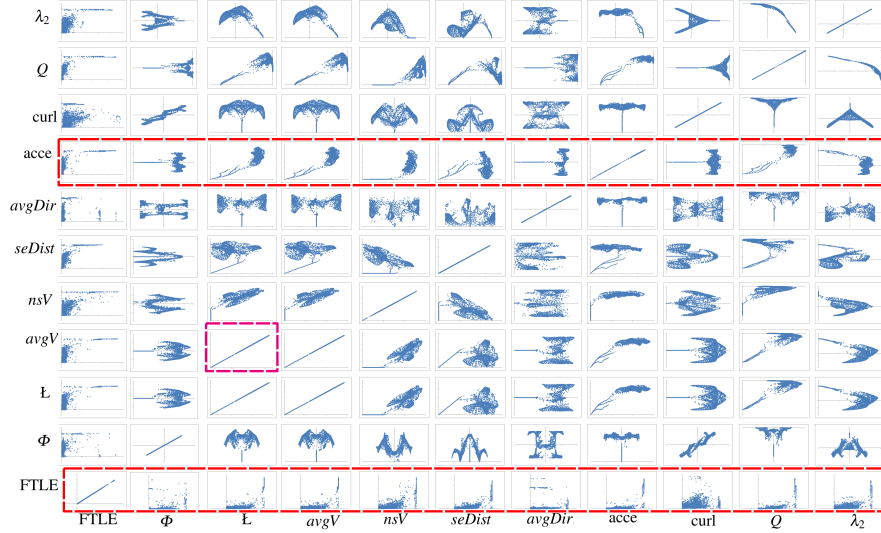
Fig. 5: The scatter plot matrix of different attribute fields of the Double Gyre flow. Note that the scatter plots associated with FTLE shows the correlation among the magnitude of the gradient of the individual attribute fields with the FTLE field.

scatter plot matrix based on the Double Gyre flow, as shown in Fig.5. Each of the entries of this matrix shows a scatter plot with two attributes as its X and Y axes. Based on this matrix, we find the following useful relations.

Length Field Ł vs. Average Particle Velocity Field $avgV$ These two attributes show a strong linear relation (entry highlighted by the purple box in the matrix). This is because the arc-length of each integral curve is equal to the sum of the velocity magnitudes, scaled by the integration step-size, measured along this curve.

Φ **vs. curl vs.** λ_2 **vs.** Q These four attributes are also closely related, as they all measure the accumulation of the amount of local flow rotation along integral curves. While Q value is always negative, the other attributes can be both positive and negative. The patterns shown in the plots $w.r.t$ Q (i.e., row Q) are generally very clear with little noise, which indicates Q could be a good attribute to consider for this data set. All the plots $w.r.t$ Φ (row Φ) and curl (row curl) exhibit certain symmetric patterns. Between these two, the plots associated with Φ tend to reveal cleaner patterns with less noise. This indicates that Φ field may be an important attribute field that encodes different flow information for subsequent data exploration.

$FTLE$ **vs. the gradient of the attribute field** The strong correlation between the gradient of the attribute fields with the $FTLE$ field is illustrated in scatter plots (row $FTLE$), as both the $FTLE$ field and the gradient operator measure the amount of change between neighboring positions. In fact it supports the discussion of the relation between the discontinuity in the attribute fields and the $FTLE$ structure in section 3.2.2 and the results of [18], i.e., the transportation structure of certain materials (e.g., some flow attributes) matches closely with the FTLE structure.

Acceleration field *aace* **vs. other attribute fields** The scatter plots of the acceleration field, which is computed by integrating the acceleration magnitude along the pathlines, and the rest attribute fields (raw *acce*) generally display clear patterns. In particular, when the value of the *acce* field is small, the other attributes tend to be small. When the value of the *acce* field is increasing and becomes large enough, the other attribute values tend to large as well. This is consistent with the knowledge that the acceleration–a result of the external force based on Newton Second Law, is the source of many different flow behaviors, such as flow separation and rotation. However, this relation is not true between *acce* and λ_2, Q. That is, the smaller the *acce* value, the larger the the absolute values of λ_2 and Q. This in fact matches the result of the work [8] that utilizes the local minima of the acceleration field to detect vortex cores.

Note that all the above discussions are based on the experiments with the Double Gyre flow. In future, we plan to further validate them with other flow datasets.

4.2 Spatial Correlation via Combined Attribute Fields

To study the spatial correlation of different attribute fields, i.e., whether they have local maxima or minima at similar locations, or whether they have similar discontinuity at the same location. , we need to perform certain spatial correlation analysis. This information cannot be easily obtained from the above scatter plots. Therefore, in the following we combine certain attribute fields of interest to define a *super attribute field*. By studying the behavior of this combined attribute field, we may obtain information about their spatial correlation. Fig. 6 provides some simple 1D examples to illustrate the logics behind the strategy of combined attribute field. If the selected attribute fields have similar behaviors (Fig. 6 upper left), the combined attribute field amplifies the similar behaviors (Fig. 6 upper right). While if selected attribute fields have different behaviors (Fig. 6 bottom left), the combined attribute weakens this difference.
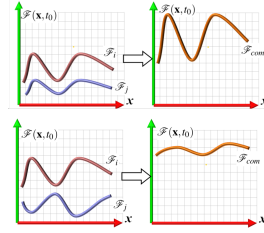

Fig. 6: The combined attribute field may strengthen the difference if the selected attributes have similar spatial behavior (upper) and vice versa (bottom).

Another reason we opt for the study of the combined attribute fields is to understand the behavior of the discontinuity in different attribute fields. To achieve that, one can simply overlap the detected edges from different attribute fields, as shown in Fig. 7(a). However, the detected edges from the individual fields are independent of each other. With this simple overlapping, it is difficult to know whether their corresponding attribute fields have similar behavior or not (i.e., both are descending, or one is descending while the other is ascending) at the places that both exhibit sharp change. This information may be revealed in the combined attribute field.

In the following, we select a pair of attribute fields to obtain the super attribute field to study their pairwise spatial correlation. Assume $\mathscr{F}_i, i = 1, 2, ..., n$ represent
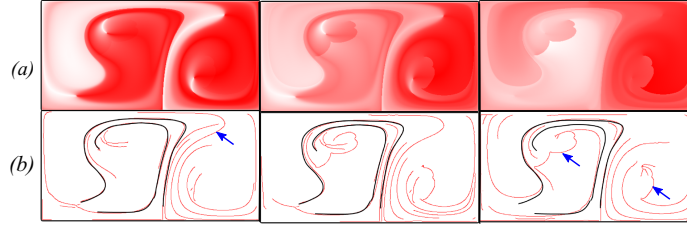
Fig. 8: Illustration of weighted combination of Φ and *avgDir* field. (a) Combined attribute field; (b) Edges detected from the super field. The dark gray curves on top are stable edges that do not change with weights. The weights of Φ and *avgDir* from let to right are $\alpha_1 = 0.1$, $\alpha_2 = 0.9$; $\alpha_1 = 0.5$, $\alpha_2 = 0.5$; $\alpha_1 = 0.9$, $\alpha_2 = 0.1$, respectively. The parameters of Canny edge detector are $\sigma = 1.0$, $\alpha = 0.3$, $\beta = 0.8$.

the attribute fields introduced in Section 3.1. We study three combination strategies to compute a super attribute field $\mathscr{F}_{com}$.

Linear combination is defined as $\mathscr{F}_{com} = \mathscr{F}_i + \mathscr{F}_j$, where $\mathscr{F}_i$ and $\mathscr{F}_j$ are selected attribute field from the attribute fields pool. However, if one of one of selected attribute field has a much larger value range, the super field will be dominated by this attribute field. Fig. 7(b) is the result of combined super field from the rotation field Φ ($[-11.73, 11.73]$) and the length field Ł ($[0., 2.8]$) , which shows mostly the features of the rotation field.

Weighted combination is employed to address the issue of the simple combination. Here, $\mathscr{F}_{com} = \alpha \widehat{\mathscr{F}_i} + \beta \widehat{\mathscr{F}_j}$, where $\alpha + \beta = 1$ and satisfies $0 \leq \alpha \leq 1, 0 \leq \beta \leq 1$. $\widehat{\mathscr{F}_i}$ and $\widehat{\mathscr{F}_j}$ are the normalized value of the attribute field $\mathscr{F}_i$ and $\mathscr{F}_j$. Fig. 8(a) shows the super fields computed using the weighted combination of the Φ and *avgDir* fields of the Double Gyre flow, with the weight for the Φ field being $0.1, 0.5$, and 0.9, respectively. With this weighted combination, we can further identify the discontinuity structure in the super field that is non-sensitive to the choices of weights. That is, no matter what weight combination is selected, the derived super field always contains this discontinuity, which we refer to as the *stable edges*. Fig. 8(b) shows this stable edge as the gray curves super-imposed onto the edges extracted

Fig. 7: (a) Overlap of edges detected from Φ (yellow) and Ł field (purple); (b) Simple combination of Φ field and Ł field.

from the corresponding super field. In this example, nine super fields, in which the weight of the Φ field is $\alpha_1 = 0.1, 0.2, ..., 0.9$, respectively, were generated to identify the stable edge.

Different from stable edges, the *common edges* indicate those edges that are exhibited by most of the attribute fields, as shown in Fig. 10 (c). Complementary to the common edges, the *unique edges* only arise in certain attribute fields. The arrow in Fig. 8(b) highlights the unique edges only possessed by the *avgDir* field and the rotation field respectively.
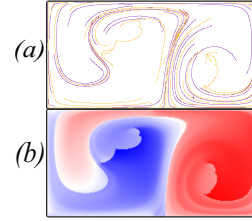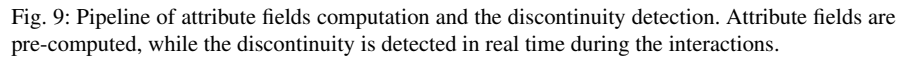
5 System Overview and Implementation

Fig. 9 shows the framework of our attribute fields based flow structure exploration. This framework consists of two main processes.

Precomputation Given the input vector field, we first compute trajectories from the sampled positions forwardly and backwardly with a user-specified time window T. The trajectories are stored as a series of spatio-temporal points. We then compute the local attributes at each spatio-temporal point along the trajectories. The attributes of these integral curves are accumulated from the local attributes and assigned to their corresponding starting points. This step can be pre-processed.

Interaction With the above pre-computed results, the user can choose to inspect the flow structure revealed by the discontinuity of a single attribute field of interest. Changing the parameters of the Canny edge detector reveals different levels of details of the structure (Fig. 4 (b-d)). The user can also choose from the list of the available attribute fields and the desired combination scheme to compute a super attribute field to study the correlation and combination of different attribute fields. Again, the Canny edge detector can be applied to reveal the discontinuity structure in the obtained super field (Fig 7 and 8).

Fig. 9: Pipeline of attribute fields computation and the discontinuity detection. Attribute fields are pre-computed, while the discontinuity is detected in real time during the interactions.

6 Results and Applications

We have applied our attribute field based analysis and exploration framework to a number of synthetic and real-world 2D vector fields. The cost of pre-computation of attribute fields depends on the resolution of the spatio-temporal domain and the time window of trajectory integration. Pathline-based attribute field computation requires 10 to 32 seconds for the data sets applied in this paper. While streakline-based attribute field computation requires about 4 to 15 minutes. All times are measured on a PC with an Intel Core i7-3537U CPU and 8GB RAM.

The first example is the Double Gyre flow with a spatial resolution of 256×128, which has been shown earlier. For the second example, we consider a dynamical system defined by the forced-damped Duffing oscillator [6]. with the constant spatial
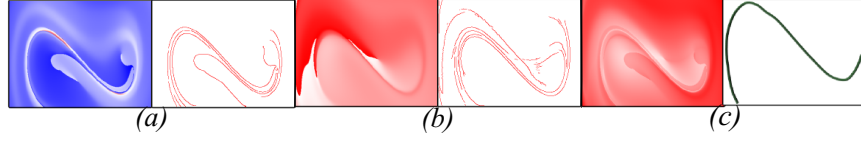
Fig. 10: Results of the forced-damped Duffing system. (a)–(b) Φ and *avgDir* fields and their detected edges. The parameters of Canny edge detector are $\sigma = 1.8$, $\alpha = 0.3$, $\beta = 0.9$. (c) A super field using the equally weighted combination of Φ, *avgDir*, *L*, *nsV* and *seDist*.
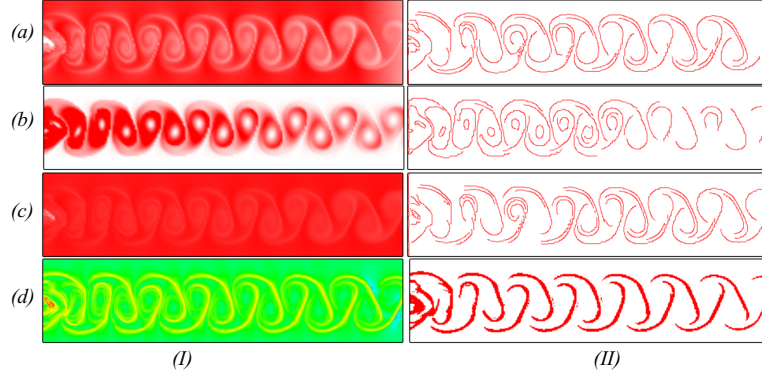

Fig. 11: Attribute fields of the flow behind cylinder and detected edges. (a) *avgV* field; (b) *nsV* field; (c) Ł field; (d) *FTLE* and LCS. The parameters of Canny edge detector are $\sigma = 1.0$, $\alpha = 0.3$, $\beta = 0.8$.

divergence operator -0.25. This system is a non-area-preserving two-dimensional dynamical system. We choose a spatial resolution of 800×600 and a time window $T = 5$. The attribute fields of the system and the corresponding detected edges are shown in Fig. 10(a). The detected edges from each attribute field encode the LCS information. Fig. 10(c) upper shows a super field combined from all the six attribute fields using weighted combination. The weight for each attribute is $\frac{1}{6}$. Fig. 10(c) bottom illustrates the detected common edges.

Another example is a simulation of a 2D unsteady flow behind a square cylinder with a Reynolds number of 160 [20]. We use a spatial resolution of 400×50 to compute the attribute fields. The time window for this data set is 3. Fig.11 shows the attribute fields and the corresponding detected edges. While the edges detected from all the attribute fields encode at least part of the LCS of the flow, the non straight velocity field *nsV* (Fig.11(b)) also reveals the swirling behavior of the flow clearly.

Our approach has the potential to reveal the cusps in spatial projection of pathlines and streaklines [21]. Fig. 12(a) shows the spatial projection of some pathlines seeded on the cusp seeding curve detected from the Φ field, while Fig. 12(b) are streaklines seeded on the singularity path extracted from a streakline-based Φ field. Both the pathlines and streaklines show cusp-like characteristics. Interestingly, the locations of cusp-like characteristic on the sample pathlines reveal the singularity path (the green dashed line in Fig. 12(a)), while those on streaklines indicate the cusp seeding curve (the green dashed curve in Fig. 12(b)). This attribute field based

discontinuity extraction we believe can be valuable for applications, such as pathline and streakline placement [21], flow domain segmentation and flow pattern search, which we will explore in future work.
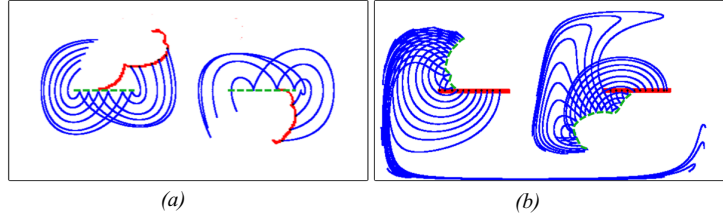

(a)   *(b)*

Fig. 12: Pathline and streakline seeding. (a) Pathlines seeded on the cusp seeding curve. (b) Streaklines seeded on the singularity path.

7 Conclusion

In this paper, we introduce a number of derived fields to encode various attributes of the integral curves. In this way, the discontinuity of the behavior of the neighboring integral curves can be studied. We show that this discontinuity may be closely related to a number of flow features. We also study different strategies to combine individual attribute fields to form a super attribute field to study the spatial correlation of the attribute fields. We integrate the attribute field computation and the discontinuity extraction to an interactive visualization system to aid the exploration of various flow structure information. In the future, we plan to extend this work to handle higher-dimensional vector fields. We also plan to have an in-depth investigation on the rigorous description between the relation of the discontinuity in these attribute fields and those well-defined flow features.

References

1. J. Canny. A computational approach to edge detection. *Pattern Analysis and Machine Intelligence, IEEE Transactions on*, (6):679–698, 1986.
2. G. Chen, K. Mischaikow, R. S. Laramee, P. Pilarczyk, and E. Zhang. Vector field editing and periodic orbit extraction using Morse decomposition. *IEEE Transactions on Visualization and Computer Graphics*, 13(4):769–785, Jul./Aug. 2007.
3. G. Chen, K. Mischaikow, R. S. Laramee, and E. Zhang. Efficient Morse decompositions of vector fields. *IEEE Transactions on Visualization and Computer Graphics*, 14(4):848–862, Jul./Aug. 2008.

4. M. Edmunds, R. S. Laramee, G. Chen, N. Max, E. Zhang, and C. Ware. Surface-based flow visualization. *Computers & Graphics*, 36(8):974–990, 2012.
5. G. Haller. Lagrangian coherent structures and the rate of strain in two-dimensional turbulence. *Phys. Fluids A*, 13:3365–3385, 2001.
6. G. Haller and T. Sapsis. Lagrangian coherent structures and the smallest finite-time lyapunov exponent. *Chaos: An Interdisciplinary Journal of Nonlinear Science*, 21(2):023115, 2011.
7. J. L. Helman and L. Hesselink. Representation and display of vector field topology in fluid flow data sets. *IEEE Computer*, 22(8):27–36, August 1989.
8. J. Kasten, J. Reininghaus, I. Hotz, and H.-C. Hege. Two-dimensional time-dependent vortex regions based on the acceleration magnitude. *Transactions on Visualization and Computer Graphics (Vis'11)*, 17(12):2080–2087, 2011.
9. K. Lu, A. Chaudhuri, T.-Y. Lee, H. W. Shen, and P. C. Wong. Exploring vector fields with distribution-based streamline analysis. In *Proceeding of PacificVis '13: IEEE Pacific Visualization Symposium*, Sydney, Australia, march 2013.
10. T. McLoughlin, M. W. Jones, R. S. Laramee, R. Malki, I. Masters, and C. D. Hansen. Similarity measures for enhancing interactive streamline seeding. *IEEE Transactions on Visualization and Computer Graphics*, 19(8):1342–1353, 2013.
11. A. Pobitzer, A. Lez, K. Matkovic, and H. Hauser. A statistics-based dimension reduction of the space of path line attributes for interactive visual flow analysis. In *Pacific Visualization Symposium (PacificVis), 2012 IEEE*, pages 113–120. IEEE, 2012.
12. A. Pobitzer, R. Peikert, R. Fuchs, B. Schindler, A. Kuhn, H. Theisel, K. Matkovic, and H. Hauser. The state of the art in topology-based visualization of unsteady flow. *Computer Graphics Forum*, 30(6):1789–1811, September 2011.
13. J. Reininghaus, C. Lowen, and I. Hotz. Fast combinatorial vector field topology. *IEEE Transactions on Visualization and Computer Graphics*, 17:1433–1443, 2011.
14. T. Salzbrunn, C. Garth, G. Scheuermann, and J. Meyer. Pathline predicates and unsteady flow structures. *The Visual Computer*, 24(12):1039–1051, 2008.
15. T. Salzbrunn and G. Scheuermann. Streamline predicates. *IEEE Transactions on Visualization and Computer Graphics*, 12(6):1601–1612, 2006.
16. S. Shadden, F. Lekien, and J. Marsden. Definition and properties of lagrangian coherent structures from finite-time lyapunov exponents in two-dimensional aperiodic flows. *Physica D*, 212(3–4):271–304, 2005.
17. K. Shi, H. Theisel, H. Hauser, T. Weinkauf, K. Matkovic, H.-C. Hege, and H.-P. Seidel. Path line attributes - an information visualization approach to analyzing the dynamic behavior of 3D time-dependent flow fields. In H.-C. Hege, K. Polthier, and G. Scheuermann, editors, *Topology-Based Methods in Visualization II*, Mathematics and Visualization, pages 75–88, Grimma, Germany, 2009. Springer.
18. K. Shi, H. Theisel, T. Weinkauf, H.-C. Hege, and H.-P. Seidel. Visualizing transport structures of time-dependent flow fields. *IEEE computer graphics and applications*, (5):24–36, 2008.
19. H. Theisel, T. Weinkauf, and H.-P. Seidel. Grid-independent detection of closed stream lines in 2D vector fields. In *Proceedings of the Conference on Vision, Modeling and Visualization 2004 (VMV 04)*, pages 421–428, Nov. 2004.
20. T. Weinkauf and H. Theisel. Streak lines as tangent curves of a derived vector field. *IEEE Transactions on Visualization and Computer Graphics (Proceedings Visualization 2010)*, 16(6):1225–1234, November - December 2010.
21. T. Weinkauf, H. Theisel, and O. Sorkine. Cusps of characteristic curves and intersection-aware visualization of path and streak lines. In R. Peikert, H. Hauser, H. Carr, and R. Fuchs, editors, *Topological Methods in Data Analysis and Visualization II*, Mathematics and Visualization, pages 161–176. Springer, 2012.
22. T. Weinkauf, H. Theisel, A. Van Gelder, and A. Pang. Stable feature flow fields. *Visualization and Computer Graphics, IEEE Transactions on*, 17(6):770–780, 2011.
23. T. Wischgoll and G. Scheuermann. Detection and visualization of closed streamlines in planar fields. *IEEE Transactions on Visualization and Computer Graphics*, 7(2):165–172, 2001.
24. H. Yu, C. Wang, C.-K. Shene, and J. H. Chen. Hierarchical streamline bundles. *IEEE Transactions on Visualization and Computer Graphics*, 18(8):1353–1367, Aug. 2012.